State Estimation For An Agonistic-Antagonistic Muscle System*

Thang Nguyen[1], Holly Warner[2], Hung La[3], Hanieh Mohammadi[1], Dan Simon[1], and Hanz Richter[2]

Abstract—**Research on assistive technology, rehabilitation, and prosthesis requires the understanding of human machine interaction, in which human muscular properties play a pivotal role. This paper studies a nonlinear agonistic-antagonistic muscle system based on the Hill muscle model. To investigate the characteristics of the muscle model, the problem of estimating the state variables and activation signals of the dual muscle system is considered. In this work, parameter uncertainty and unknown inputs are taken into account for the estimation problem. Three observers are presented: a high gain observer, a sliding mode observer, and an adaptive sliding mode observer. Theoretical analysis shows the convergence of the three observers. To facilitate numerical simulations, a backstepping controller is employed to drive the muscle system to track a desired trajectory. Numerical simulations reveal that the three observers are comparable and provide reliable estimates in noise free and noisy cases. The proposed schemes may serve as frameworks for estimation of complex multi-muscle systems, which could lead to intelligent exercise machines for adaptive training and rehabilitation, and adaptive prosthetics and exoskeletons.**

Index Terms—**Hill muscle model, human muscles, state estimation, sliding mode observer, adaptive sliding mode, high gain observer.**

I. INTRODUCTION

The development of robotics research has facilitated studies on applications in assisting human in various scenarios, see [1], [2] and references therein. In [1], improved functionality in persons with certain neurological disorders was addressed. In [3], human-like mechanical impedance based on the simulation of the models of the human neuromuscular system was studied. In [4], several virtual agonist-antagonist muscle mechanisms were considered in control of multilegged animal walking, where the controller is a combination of neural control with tunable muscle-like functions. In [5], the estimation of joint force using a biomechanical muscle model and peaks of surface electromyography was studied.

The design of prosthetic, orthotic, and functional neuromuscular stimulation systems requires the understanding of the coordination of the human body and the dynamical properties of muscles [6]. The intermuscular coordination can be studied based on classical models proposed by Hill, Wilkie, and Richie [6]. The most widely implemented model for simulating human muscles is the Hill model [7]. More complicated models, including partial differential equation [8] or finite element [9] models, have been introduced to capture the complex behavior of human muscles. For a balance between accuracy and computational realizability, the Hill muscle model is a prominent solution [6].

Human muscles operate at many joints. For a given joint, muscles often act in pairs with one or more muscles on opposite sides. Each member of a pair is regarded as agonist or antagonist. In this paper, an agonistic-antagonistic muscle system based on the Hill muscle model is introduced to study coordination and estimate muscle parameters. The agonistic-antagonistic muscle system is scalable in the sense that its dynamic behavior and characteristics can be extended to multi-joint, multi-muscle, and 3D systems. In [10], muscular activities of a dominant antagonistic muscle pair are employed to address a computationally efficient model of the arm endpoint stiffness behavior.

A variety of estimation problems for different muscle models have been addressed. In [11], muscle forces, joint moments, and/or joint kinematics are estimated from electromyogram signals using forward dynamics. In [12], the estimation problem of individual muscle forces during human movement is solved using forward dynamics. In [13], the muscular torque is estimated using a nonlinear observer in a sliding mode controller of a human-driven knee joint orthosis. In [14], the estimation of muscle activity is conducted using higher-order derivatives, static optimization, and forward-inverse dynamics. In [15], an inverse dynamic optimization problem is proposed to estimate muscle and contact forces in the knee during gait. In [16], the trajectory tracking control problem of one-degree of freedom manipulator system driven by a pneumatic artificial muscle is addressed, in which a novel extended state observer based on a generalized super-twisting algorithm is employed to deal with internal uncertainties and external disturbances.

There have been numerous estimation methods proposed to observe nonlinear systems, from high gain observers to sliding mode observers; see [17]–[25] and references therein. High gain observers can offer a high level of accuracy in estimating state variables and uncertainties [22], [23], [25]. Sliding mode observers exhibit similar performance in estimating state variables and unknown inputs [18], [20], [21], [24]. Therefore, sliding mode observers, which are based on sliding mode control, can be employed to address many problems in fault detection and isolation, in which important parameters such as state variables, faults or unknown inputs need to be reconstructed from the available information. While traditional sliding mode techniques require the knowledge of unknown inputs and uncertainties, recent adaptive sliding mode control

[1] Department of Electrical Engineering and Computer Science, Cleveland State University, Cleveland, Ohio 44115, USA

[2] Department of Mechanical Engineering, Cleveland State University, Cleveland, Ohio 44115, USA

[3] Advanced Robotics and Automation (ARA) Lab, Department of Computer Science and Engineering, University of Nevada, Reno, NV 89557, USA

methods have been developed to overcome this limit at the cost of complexity [26], [27].

Muscle systems are important in assistive technology, rehabilitation, and prosthesis related research, which involves human-machine interactions. In this paper, we aim to design a high gain observer, a conventional sliding mode observer, and a new adaptive sliding mode observer for our dual muscle system. The benefits of accurate state estimation for the agonistic-antagonistic muscle model offer useful frameworks to investigate several problems in human-machine interactions such as monitoring of human health state and gait analysis [28]–[30], 3-D human skeleton localization [31], human foot localization [32], [33], artificial muscles [16], etc.

The contribution of our research work lies in the construction and development of a high gain observer, a sliding mode observer, and an adaptive sliding mode observer for the agonistic-antagonistic muscle system where unknown inputs are taken into account. Our problem is more general than the works in [16], [25], in which unknown input estimation is not considered, and more general than [24], where modeling uncertainties are not taken into account. The high gain observer is designed based on recent results in [22], [23], which allows to estimate state variables and unknown inputs, from which activation signals are constructed. The conventional sliding mode observer is built based on the first order sliding mode and super-twisting algorithm developed in [19], [34], for which bounds of unknown control inputs and uncertainty needs to be known. The third observer is developed based on recent results on dual layer adaptive sliding mode control [26], [27], which does not require knowledge of the bounds of unknown inputs and uncertainty.

The rest of the paper is organized as follows. Section II presents the problem formulation. Section III introduces three observers to estimate state variables and activation signals. Section IV shows numerical simulations to demonstrate the effectiveness of the proposed schemes, where Subsection IV-A presents a backstepping controller for the tracking control problem. Section V concludes the paper.

II. PROBLEM FORMULATION

We study the agonistic-antagonistic muscle system where each muscle is based on the Hill muscle model [6]. The Hill muscle unit models several effects of the physical muscle. It is divided into two sections, the tendon and the muscle body. The tendon is modeled as a nonlinear stiffness that includes some amount of slack. Within the muscle body portion of the model, a nonlinear stiffness element, modeled similar to the tendon, and a force generation element are oriented in parallel. The tendon and muscle body components are then placed in series. The structure of the dual muscle system is described in Fig. 1, where the abbreviations *CE*, *SEE*, and *PE* stand for the contractile, series elastic, and parallel elastic elements of the Hill muscle model. Because muscles can only apply force when contracting, two muscles are required to actuate the central mass m, which is a simple load selected for studying the fundamental dynamics of this system.
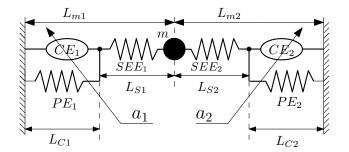

Fig. 1. Two-muscle, one degree-of-freedom agonistic-antagonistic system with mass load [35].

The lengths of the *CE* and *SEE* are denoted as L_{Cj} and L_{Sj} for muscle j ($j = 1, 2$), and the total length of the jth muscle is defined by

$$L_{mj} = L_{Cj} + L_{Sj}. \tag{1}$$

Let L_{m1} be the position of the mass in Fig. 1, and the corresponding velocity is positive to the right.

The dual muscle system possesses the following dynamics [35], [36]

$$\dot{x}_1 = x_2 \tag{2}$$
$$\dot{x}_2 = \frac{1}{m}(\Phi_{S2}(L_{S2}) - \Phi_{S1}(L_{S1})) + \Delta_\Phi(\tau) \tag{3}$$
$$\dot{L}_{S1} = x_2 + g_1^{-1}(z_1) \tag{4}$$
$$\dot{L}_{S2} = -x_2 + g_2^{-1}(z_2) \tag{5}$$

where

$$x_1 \triangleq L_{m1}, \tag{6}$$
$$z_j = \frac{\Phi_{Sj}(L_{Sj}) - \Phi_{Pj}(L_{Cj})}{a_j f_j(L_{Cj})} \text{ for } j = 1, 2, \tag{7}$$

where Φ_{Sj} is the elastic force, Φ_{Pj} is the parallel elastic force, a_j is the activation signal of element j with $a_j \in [0, 1]$, and $\Delta_\Phi(\tau)$ is a bounded uncertainty. The force-length dependence factor f_j has the general shape of a Gaussian curve, and the velocity dependence function $g_j^{-1}(z_j)$ obeys the Hill model:

$$f_j(L_{Cj}) = exp[-\left(\frac{L_{Cj} - 1}{W}\right)^2] \tag{8}$$

$$g_j^{-1}(z_j) = \begin{cases} \dfrac{1 - z_j}{1 + z_j/A}, & z_j \leq 1 \\ \dfrac{-A(z_j - 1)(g_{max} - 1)}{(A + 1)(g_{max} - z_j)}, & z_j > 1 \end{cases} \tag{9}$$

where W, A, and g_{max} are positive parameters. Denote

$$u_1 \triangleq g_1^{-1}(z_1) \tag{10}$$
$$u_2 \triangleq g_2^{-1}(z_2) \tag{11}$$

as the virtual control inputs of the system (2), (3), (4), (5).

We have the following assumptions for our system.

Assumption 2.1: The uncertainty $\Delta_\Phi(\tau)$ satisfies

$$|\Delta_\Phi(\tau)| < \Delta_m \tag{12}$$

where Δ_m is a positive constant.

Remark 2.1: $\Delta_\Phi(\tau)$ can represent parameter uncertainties due to model mismatch. For example, uncertainties in the description of $\Phi_{Sj}(L_{Sj})$ and the mass m.

Assumption 2.2: The control inputs of the system (2), (3), (4), (5) satisfy

$$|u_j(\tau)| < U_{jm} \text{ for } j = 1, 2 \tag{13}$$

where U_{jm} is a positive constant.

The length constraint of the dual muscle system is given by

$$L_{m1} + L_{m2} = C \tag{14}$$

where C is a constant. Hence, L_{C1} and L_{C2} will be determined from the relations in (1) and (14) if C, L_{S1}, L_{S2}, and L_{m1} are available. Therefore, it is sufficient to consider four differential equations of the model in (2), (3), (4), and (5) for our estimation problem. From (1), (4), (5), and (14), the dynamics of L_{C1} and L_{C2} are described as

$$\dot{L}_{C1} = -g_1^{-1}(z_1) \tag{15}$$
$$\dot{L}_{C2} = -g_2^{-1}(z_2). \tag{16}$$

The nonlinear functions Φ_{Sj}, Φ_{Pj}, f_j, and g_j^{-1} ($j = 1, 2$) can be found in [35], [36]. All the variables and functions of the dual muscle system are normalized to simplify the dynamics. A candidate of $\Phi_{Sj}(L_{Sj})$ is chosen as [36]

$$\Phi_{Sj}(L_{Sj}) =$$
$$\begin{cases} 0 & L_{Sj} < 2 \\ 6760794.14(L_{Sj})^5 - 68434261.19(L_{Sj})^4 \\ +277072371.99(L_{Sj})^3 - 560875494.46(L_{Sj})^2 \\ +567666340.97(L_{Sj}) - 229806913.40 & 2 \le L_{Sj} < 2.04 \\ 0.5 + 19.2308(L_{Sj} - 2.04) & L_{Sj} \ge 2.04 \end{cases}$$
$$\tag{17}$$

whose graph is shown in Fig. 2. This function has the general shape of the tendon force-length characteristic, including slack. The piecewise polynomial in the expression of $\Phi_{Sj}(L_{Sj})$ is continuous up to the second derivative. An example of Φ_{Pj} is given as [36]

$$\Phi_{Pj}(L_{Cj}) = \begin{cases} 0, & L_{Cj} < 1 \\ 8(L_{Cj})^3 - 24(L_{Cj})^2 + 24 L_{Cj} - 8, & L_{Cj} \ge 1. \end{cases}$$
$$\tag{18}$$

Remark 2.2: The function $\Phi_{Sj}(L_{Sj})$ in (17) is just one possibility to capture the stress-strain curve of a tendon. The shape of $\Phi_{Sj}(L_{Sj})$ can be built from data extracted from experiments. Note that the exact shape of $\Phi_{Sj}(L_{Sj})$ is not important as long as this function is known to controllers and observers.

Assume that x_1, $\Phi_{S1}(L_{S1})$, and $\Phi_{S2}(L_{S2})$ are available for measurement. The mass position can be tracked by a sensor while the *SEE* nonlinear spring forces $\Phi_{S1}(L_{S1})$ and $\Phi_{S2}(L_{S2})$ of the agonistic-antagonistic muscles can be measured by two load cells, from which L_{Sj} is inferred due to the inverse of $\Phi_{Sj}(L_{Sj})$. The observability matrix of the dual muscle system can be calculated using the Lie derivatives of the outputs, and it has rank 4, implying that the dual muscle system is locally observable [37].
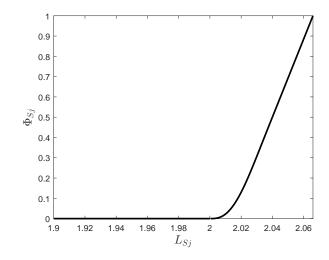
For ease of presentation, let

Fig. 2. The graph of function Φ_{Sj} described in (17).

$$x_3 \triangleq L_{S1} \tag{19}$$
$$x_4 \triangleq L_{S2}. \tag{20}$$

Due to the relations (1) and (14), L_{Cj} can be deduced from L_{mj} and L_{Sj}. Our system is rewritten as

$$\dot{x}_1 = x_2 \tag{21}$$
$$\dot{x}_2 = \frac{1}{m}(\Phi_{S2}(x_4) - \Phi_{S1}(x_3)) + \Delta_\Phi(\tau) \tag{22}$$
$$\dot{x}_3 = x_2 + u_1(x) \tag{23}$$
$$\dot{x}_4 = -x_2 + u_2(x) \tag{24}$$
$$y_1 = x_1 \tag{25}$$
$$y_2 = \Phi_{S1}(x_3) \tag{26}$$
$$y_3 = \Phi_{S2}(x_4) \tag{27}$$

where

$$x = \begin{bmatrix} x_1 \\ x_2 \\ x_3 \\ x_4 \end{bmatrix}, \tag{28}$$

and the vector

$$y = \begin{bmatrix} y_1 \\ y_2 \\ y_3 \end{bmatrix} \tag{29}$$

is the output of the dual muscle system. Note that from the measurement of y_2 and y_3, x_3 and x_4 can be calculated due to the inverse of the function $\Phi_{Sj}(L_{Sj})$ in (17). Let

$$u = \begin{bmatrix} u_1 \\ u_2 \end{bmatrix}. \tag{30}$$

Given the measurements of the length of the agonistic muscle and muscle forces, we study the estimation problem of state and activation signals. Due to the relation (7), it is sufficient to estimate the state and unknown inputs of the system (21) - (27).

III. OBSERVER DESIGN

In this section, we introduce three methods to estimate the state variables and the activation signals: a high gain observer, a sliding mode observer, and an adaptive sliding observer. Denote the estimates of x, u, and $a = [a_1, a_2]^T$ as

$$\hat{x} = \begin{bmatrix} \hat{x}_1 \\ \hat{x}_2 \\ \hat{x}_3 \\ \hat{x}_4 \end{bmatrix} \tag{31}$$

$$\hat{u} = \begin{bmatrix} \hat{u}_1 \\ \hat{u}_2 \end{bmatrix} \tag{32}$$

$$\hat{a} = \begin{bmatrix} \hat{a}_1 \\ \hat{a}_2 \end{bmatrix}. \tag{33}$$

A. HIGH GAIN OBSERVER

The high gain observer in this subsection is designed based on the extended high gain observer approach reported in [22], [23]. The structure of the proposed high gain observer is described as

$$\dot{\hat{x}}_1 = \hat{x}_2 + \frac{h_{11}}{\varepsilon_h}(y_1 - \hat{x}_1) \tag{34}$$

$$\dot{\hat{x}}_2 = \frac{1}{m}(y_3 - y_2) + \hat{\Delta}_\Phi(t) \\ + \frac{h_{12}}{\varepsilon_h^2}(y_1 - \hat{x}_1) \tag{35}$$

$$\dot{\hat{\Delta}}_\Phi = \frac{h_{13}}{\varepsilon_h^3}(y_1 - \hat{x}_1) \tag{36}$$

$$\dot{\hat{x}}_3 = \hat{x}_2 + \hat{u}_1 + \frac{h_{21}}{\varepsilon_h}(\Phi_{S1}^{-1}(y_2) - \hat{x}_3) \tag{37}$$

$$\dot{\hat{u}}_1 = \frac{h_{22}}{\varepsilon_h^2}(\Phi_{S1}^{-1}(y_2) - \hat{x}_3) \tag{38}$$

$$\dot{\hat{x}}_4 = -\hat{x}_2 + \hat{u}_2 + \frac{h_{31}}{\varepsilon_h}(\Phi_{S2}^{-1}(y_3) - \hat{x}_4) \tag{39}$$

$$\dot{\hat{u}}_2 = \frac{h_{32}}{\varepsilon_h^2}(\Phi_{S2}^{-1}(y_3) - \hat{x}_4), \tag{40}$$

where $\varepsilon_h \in (0,1)$ is a design parameter, parameters h_{11}, h_{12}, h_{13} are chosen such that the polynomial $s^3 + h_{11}s^2 + h_{12}s + h_{13}$ is Hurwitz, parameters h_{ij} for $i = 2,3$ and $j = 1,2$ are chosen such that the polynomials $s^2 + h_{i1}s + h_{i2}$ are Hurwitz for $i = 2,3$ [22].

Theorem 3.1: Under Assumptions 2.1 and 2.2, the state and input estimates of the high gain observer presented in (34) - (40) satisfy

$$\|x(\tau) - \hat{x}(\tau)\| \to 0 \tag{41}$$

and

$$\|u_j(\tau) - \hat{u}_j(\tau)\| \to 0 \text{ for } j = 1,2 \tag{42}$$

as $\varepsilon_h \to 0$ for $\tau \geq 0$.
Proof: The proof is based on the construction of the extended high gain observer in [22], [23]. ∎

Remark 3.1: Theorem 3.1 states that if $\varepsilon_h \to 0$, the state and unknown input estimates will be exactly the true values. Since $\varepsilon_h \neq 0$, a practical choice of ε_h lies in the interval $(0,1)$.

Remark 3.2: The proposed high gain observer requires the tuning of nine parameters: ε_h, h_{11}, h_{12}, h_{13}, h_{21}, h_{22}, h_{31}, h_{32}.

B. SLIDING MODE OBSERVER

Following the super twisting algorithm and the traditional sliding mode approach in [19], [34], the sliding mode observer for our system possesses the following structure:

$$\dot{\hat{x}}_1 = \hat{x}_2 + v_{11} \tag{43}$$

$$\dot{\hat{x}}_2 = \frac{1}{m}(y_3 - y_2) + v_{12} \tag{44}$$

$$\dot{\hat{x}}_3 = \hat{x}_2 + v_2 \tag{45}$$

$$\dot{\hat{x}}_4 = -\hat{x}_2 + v_3 \tag{46}$$

where

$$v_{11} = \lambda_{11}|y_1 - \hat{x}_1|^{1/2}\text{sign}(y_1 - \hat{x}_1) \tag{47}$$

$$v_{12} = \alpha_{11}\text{sign}(y_1 - \hat{x}_1) \tag{48}$$

$$v_2 = \alpha_2\text{sign}(\Phi_{S1}^{-1}(y_2) - \hat{x}_3) \tag{49}$$

$$v_3 = \alpha_3\text{sign}(\Phi_{S2}^{-1}(y_3) - \hat{x}_4). \tag{50}$$

Here λ_{11} and α_{11} are design parameters which can be chosen to satisfy the following inequalities [19]:

$$\alpha_{11} > f^+ \tag{51}$$

$$\lambda_{11} > \sqrt{\frac{2}{\alpha_{11} - f^+}}\frac{(\alpha_{11} + f^+)(1+p)}{(1-p)} \tag{52}$$

where p is a positive constant such that $0 < p < 1$, $f^+ > 0$ is the upperbound of Δ_Φ: $|\Delta_\Phi| < f^+$. The parameters λ_{11} and α_{11} can also be taken according to [38]. The parameters α_2 and α_3 in (49) and (50) are chosen such that [34]

$$U_{1m} < \alpha_2 \tag{53}$$

$$U_{2m} < \alpha_3 \tag{54}$$

where U_{1m} and U_{2m} are defined in (13). The reconstruction of the uncertainty Δ_Φ and unknown inputs u_1 and u_2 is accomplished with low pass filters given as

$$\tau_s\dot{\hat{\Delta}}_\Phi = -\hat{\Delta}_\Phi + v_{12} \tag{55}$$

$$\tau_s\dot{\hat{u}}_1 = -\hat{u}_1 + v_2 \tag{56}$$

$$\tau_s\dot{\hat{u}}_2 = -\hat{u}_2 + v_3 \tag{57}$$

where τ_s is a positive parameter.

We have the following result.

Theorem 3.2: Under Assumptions 2.1 and 2.2, there exists a positive number $\tau^\star$ such that the state and input estimates of the high gain observer presented in (43) - (46) and (55) - (57) satisfy

$$x(\tau) - \hat{x}(\tau) = 0 \tag{58}$$

and

$$u(\tau) \to \hat{u}(\tau) \tag{59}$$

for $\tau \geq \tau^\star$.
Proof: The proof follows the super-twisting algorithm and the standard sliding mode in [19], [34]. Let

$$e = x - \hat{x}. \tag{60}$$

The state estimation dynamics are

$$\dot{e}_1 = e_2 - v_{11} \tag{61}$$
$$\dot{e}_2 = \Delta_\Phi(\tau) - v_{12} \tag{62}$$
$$\dot{e}_3 = e_2 + u_1 + v_2 \tag{63}$$
$$\dot{e}_4 = -e_2 + u_2 + v_3. \tag{64}$$

According to [19], there exists a number $\tau_1^\star > 0$ such that $e_1(\tau) = 0$ and $e_2(\tau) = 0$ for $\tau \geq \tau_1^\star$. It is easy to show that e_3 and e_4 are bounded in the interval $[0, \tau_1^\star]$. Since the error dynamics of e_3 is the first order sliding mode for $\tau \geq \tau_1^\star$, there exists a number $\tau_2^\star \geq \tau_1^\star$ such that $e_3(\tau) = 0$ for $\tau \geq \tau_2^\star$ [34]. Using the same argument, there exists a number $\tau_3^\star \geq \tau_1^\star$ such that $e_4(\tau) = 0$ for $\tau \geq \tau_3^\star$. Therefore, $e = 0$ for $\tau \geq \tau^\star = \max\{\tau_1^\star, \tau_2^\star, \tau_3^\star\}$.

According to [19], [34], the injection signals v_{12}, v_2, and v_3 are employed to estimate Δ_Φ, u_1, and u_2 in (55), (56), (57), from which $\hat{\Delta}_\Phi \to \Delta_\Phi$ and $\hat{u} \to u$. ∎

Remark 3.3: A practical implementation of the sign function of the sliding mode observer is done using the following approximation:

$$\text{sign}(e) \approx \frac{e}{\delta_s + |e|}, \tag{65}$$

which adds another design parameter for the observer, namely δ_s.

Remark 3.4: The proposed sliding mode observer requires the tuning of six parameters: λ_{11}, α_{11}, α_2, α_3, τ_s, δ_s.

Remark 3.5: The parameters of the sliding mode observer depend explicitly on the information of the bounds of the unknown inputs and uncertainty.

C. ADAPTIVE SLIDING MODE OBSERVER

The adaptive sliding mode observer for our system is designed based on the dual layer nested adaptive approaches in [26], [27]. The proposed adaptive sliding mode observer is given as follows:

$$\dot{\hat{x}}_1 = \hat{x}_2 + \alpha_a(\tau)|y_1 - \hat{x}_1|^{1/2}\text{sign}(y_1 - \hat{x}_1) - \phi(y_1 - \hat{x}_1, L_a) \tag{66}$$
$$\dot{\hat{x}}_2 = \beta_a(\tau)\text{sign}(y_1 - \hat{x}_1) \tag{67}$$
$$\dot{\hat{\Delta}}_\Phi = \frac{1}{\tau_a}(-\hat{\Delta}_\Phi - \beta_a(\tau)\text{sign}(y_1 - \hat{x}_1)) \tag{68}$$
$$\dot{\hat{x}}_3 = (k_1(\tau) + \eta_1)\text{sign}(\Phi_{S1}^{-1}(y_2) - \hat{x}_3) \tag{69}$$
$$\dot{\hat{u}}_1 = \frac{1}{\tau_a}(-\hat{u}_1 - (k_1(\tau) + \eta_1)\text{sign}(\Phi_{S1}^{-1}(y_2) - \hat{x}_3)) \tag{70}$$
$$\dot{\hat{x}}_4 = (k_2(\tau) + \eta_2)\text{sign}(\Phi_{S2}^{-1}(y_3) - \hat{x}_4) \tag{71}$$
$$\dot{\hat{u}}_2 = \frac{1}{\tau_a}(-\hat{u}_2 - (k_2(\tau) + \eta_2)\text{sign}(\Phi_{S2}^{-1}(y_3) - \hat{x}_4)) \tag{72}$$

where τ_a, η_1, and η_2 are positive design parameters,

$$\alpha_a(\tau) = \sqrt{L_a(\tau)}\,\alpha_0 \tag{73}$$
$$\beta_a(\tau) = L_a(\tau)\beta_0, \tag{74}$$

where α_0 and β_0 are fixed positive scalars and

$$\phi(e_1, L_a) = -\frac{\dot{L}_a(\tau)}{L_a(\tau)} e_1(\tau). \tag{75}$$

Define

$$\delta_{a0}(\tau) = L_a(\tau) - \frac{1}{a\beta_0}|\hat{\Delta}_\Phi| - \varepsilon_a \tag{76}$$

where a is chosen such that $0 < a < 1/\beta_0 < 1$ and ε_a is a small positive scalar chosen to satisfy

$$\frac{1}{a\beta_0}|\hat{\Delta}_\Phi| + \varepsilon_a/2 > |\Delta_\Phi|. \tag{77}$$

The proposed adaptive element $L_a(\tau)$ is given by

$$L_a(\tau) = l_0 + l_a(\tau) \tag{78}$$

where l_0 is a small positive design constant and

$$\dot{l}_a(\tau) = -\rho_{a0}(\tau)\text{sign}(\delta_a(\tau)). \tag{79}$$

The time-varying term in (79) is given by

$$\rho_{a0}(\tau) = r_{00} + r_{a0}(\tau) \tag{80}$$

where r_{00} is a positive design parameter,

$$\dot{r}_{a0}(\tau) = \begin{cases} \gamma_{a0}|\delta_{a0}(\tau)| & \text{if } |\delta_{a0}(\tau)| > \delta_{00} \\ 0 & \text{otherwise} \end{cases} \tag{81}$$

where δ_{a0} is defined in (76), $\gamma_{a0} > 0$ and $\delta_{00} > 0$ are design parameters. For $j = 1, 2$, define

$$\delta_{aj}(\tau) = k_j(\tau) - \frac{1}{\alpha_{aj}}|\hat{u}_j| - \varepsilon_{aj} \tag{82}$$

where α_{aj} is chosen such that $0 < \alpha_{aj} < 1$ and $\varepsilon_{aj} > 0$ is a small positive scalar chosen to satisfy

$$\frac{1}{\alpha_{aj}}|\hat{u}_j| + \varepsilon_{aj}/2 > |u_j|. \tag{83}$$

The proposed adaptive elements $k_j(\tau)$ are given by

$$\dot{k}_j(\tau) = -\rho_{aj}(\tau)\text{sign}(\delta_{aj}(\tau)) \tag{84}$$

for $j = 1, 2$. The time-varying terms in (84) are given by

$$\rho_{aj}(\tau) = r_{0j} + r_{aj}(\tau), \text{ for } j = 1, 2 \tag{85}$$

where

$$\dot{r}_{aj}(\tau) = \begin{cases} \gamma_{aj}|\delta_{aj}(\tau)| & \text{if } |\delta_{aj}(\tau)| > \delta_{0j} \\ 0 & \text{otherwise} \end{cases} \tag{86}$$

where $\gamma_{aj} > 0$ and δ_{0j} is a small positive parameter.

Theorem 3.3: Under Assumptions 2.1 and 2.2, there exists a positive number $\tau^\dagger$ such that the state and input estimates of the high gain observer presented in (66) - (72) satisfy

$$x(\tau) - \hat{x}(\tau) = 0 \tag{87}$$

and

$$u(\tau) \to \hat{u}(\tau) \tag{88}$$

for $\tau \geq \tau^\dagger$.

Proof: The proof follows the results of the dual layer nested adaptive approaches in [26], [27]. The error dynamics for the state estimation are

$$\dot{e}_1 = e_2 - \alpha_a(\tau)|e_1|^{1/2}\text{sign}(e_1) - \phi(e_1, L_a) \tag{89}$$
$$\dot{e}_2 = \Delta_\Phi - \beta_a(\tau)\text{sign}(e_1) \tag{90}$$
$$\dot{e}_3 = e_2 - (k_1(\tau) + \eta_1)\text{sign}(e_3) \tag{91}$$
$$\dot{e}_4 = -e_2 - (k_2(\tau) + \eta_2)\text{sign}(e_4). \tag{92}$$

According to [27], there exists a number $\tau_1^\dagger > 0$ such that $e_1(\tau) = 0$ and $e_2(\tau) = 0$ for $\tau \geq \tau_1^\dagger$. It is easy to show that e_3 and e_4 are bounded in the interval $[0, \tau_1^\dagger]$.

According to [26], there exists a number $\tau_2^\dagger \geq \tau_1^\dagger$ such that $e_3(\tau) = 0$ for $\tau \geq \tau_2^\dagger$ [34]. Using the same argument, there exists a number $\tau_3^\dagger \geq \tau_1^\dagger$ such that $e_4(\tau) = 0$ for $\tau \geq \tau_3^\dagger$. Therefore, $e = 0$ for $\tau \geq \tau^\dagger = \max\{\tau_1^\dagger, \tau_2^\dagger, \tau_3^\dagger\}$.

The recovery of Δ_Φ, u_1, and u_2 follows the standard filtering approach in sliding mode control [34] in (68), (70), (72), from which $\hat{\Delta}_\Phi \to \Delta_\Phi$ and $\hat{u} \to u$. ∎

Remark 3.6: Similar to the traditional sliding mode observer, the sign function of the adaptive sliding mode observer can be approximated using the expression in (65)

$$\text{sign}(e) \approx \frac{e}{\delta_a + |e|}, \tag{93}$$

which introduces another design parameter, that is δ_a.

Remark 3.7: The proposed adaptive sliding mode observer requires the tuning of 21 parameters: α_0, β_0, η_1, η_2, a, l_0, r_{00}, r_{01}, r_{02}, τ_a, ε_{a1}, ε_{a2}, α_{a1}, α_{a2}, γ_{a0}, γ_{a1}, γ_{a2}, δ_{00}, δ_{01}, δ_{02}, δ_a.

Remark 3.8: The parameters of the adaptive sliding mode observer in general do not depend on the bounds of the unknown inputs and uncertainty.

IV. NUMERICAL EXAMPLE

For the purpose of estimation, we employ a backstepping controller for the output L_{m1} to track a time-varying reference signal. A numerical example will be conducted using the proposed controller and observers to estimate the state variables and the activation signals.

A. BACKSTEPPING CONTROLLER

The specific controller is irrelevant for estimation analysis and design, as long as the estimates are not being fed back to the controller. This is the case even when the estimator does not have access to direct control input measurements, provided an accurate dynamic model is available.

In this paper, a tracking control scheme is constructed based on its counterpart for setpoint regulation [35]. A tracking extension for the dual muscle system, which includes activation dynamics, is reported in [39]. A control method based on an artificial field approach can be derived as in [40]. Our goal is to design a stable feedback tracking controller for the position of the mass, in which u_1 and u_2 are control inputs. The activation signals a_1 and a_2 are subsequently calculated from the relation in (6). Assume that the uncertainty Δ_Φ is known to the controller.

As in [35], the standard backstepping procedure is employed to synthesize a virtual control input based on tendon force difference to setpoint-stabilize the load subsystem formed by (2) and (3). The constructive scheme is based on a Lyapunov function V that becomes negative-definite for the load subsystem under the synthetic control law.

In [35], two alternative methods for the synthetic input are employed: a scalar approach and a vector approach. We aim to design our control method based on the former. Denote

the reference signal as $r(t)$ and assume that it is twice differentiable.

Denote the tracking error and its derivative as

$$e = \begin{bmatrix} e_1 \\ e_2 \end{bmatrix} = \begin{bmatrix} x_1 - r \\ \dot{x}_1 - \dot{r} \end{bmatrix}. \tag{94}$$

Furthermore, define

$$\zeta = \Phi_{S2}(L_{S2}) - \Phi_{S1}(L_{S1}) + m\Delta_\Phi - m\dot{r}. \tag{95}$$

Our goal is to design u_1 and u_2 such that e converges to 0. The error dynamics is described in the form

$$\dot{e} = Ae + B\zeta \tag{96}$$

where

$$A = \begin{bmatrix} 0 & 1 \\ 0 & 0 \end{bmatrix}, \quad B = \begin{bmatrix} 0 \\ \frac{1}{m} \end{bmatrix}. \tag{97}$$

Consider the Lyapunov function

$$V = \frac{1}{2} e^T P e \tag{98}$$

where P is a positive definite matrix. The system (96) is stable if a state feedback regulator is chosen as $\zeta = \Psi(e) = -Ke$ such that $A_{cl} = A - BK$ is Hurwitz. Hence,

$$\dot{V} = \frac{1}{2} e^T (A_{cl}^T P + P A_{cl}) e = -\frac{1}{2} e^T Q e \tag{99}$$

where Q is positive definite. Thus, $\dot{V} < 0$. This implies that the error converges to 0. However, ζ is not a direct control input. As a result, we introduce a variable

$$w = \zeta - \Psi(e). \tag{100}$$

Its derivative is given as

$$\dot{w} = \dot{\zeta} - \dot{\Psi}(e) = \Phi'_{S2}\dot{L}_{S2} - \Phi'_{S1}\dot{L}_{S1} + m\dot{\Delta}_\Phi - m\ddot{r} \tag{101}$$

where

$$\Phi'_{Si} = \frac{d\Phi_{Si}}{dL_{Si}} \tag{102}$$

for $i = 1, 2$. The error dynamics is rewritten as

$$\dot{e} = A_{cl}e + Bw \tag{103}$$

Augment the Lyapunov function V with a quadratic term in w

$$V_a = V + \frac{1}{2} w^2. \tag{104}$$

Taking its derivative yields

$$\dot{V}_a = -\frac{1}{2} e^T Q e + w\kappa \tag{105}$$

where

$$\kappa = \Phi'_{S2}(x_2 + u_2) - \Phi'_{S1}(-x_2 + u_1) + m\dot{\Delta}_\Phi - m\ddot{r} + B^T P e. \tag{106}$$

Here, κ is chosen such that $\kappa = -\gamma w$ with $\gamma > 0$ to make $\dot{V}_a$ negative definite. Hence, the augmented system of e and w is asymptotically stable. It should be noted that we cannot deduce unique solutions of u_1 and u_2 from κ in (106).

From (106),

$$\Phi'_{S2}u_2 - \Phi'_{S1}u_1 = \beta \tag{107}$$

where

$$\beta = -K_1\zeta - K_2e - (\Phi'_{S2} + \Phi'_{S1})x_2 + m\ddot{r}$$
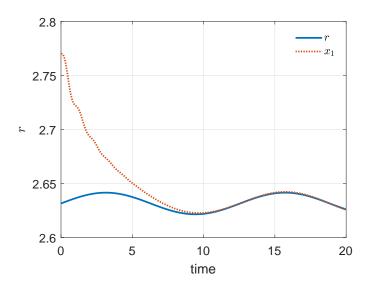
Fig. 3. The reference signal r and the output $y_1 = x_1$. All quantities are dimensionless (no units).

with $K_1 = \gamma + KB$, and $K_2 = (KA + \gamma K + B^T P)e$. The control redundancy can be resolved using the least square solution to (107), which solves the minimization of $u_1^2 + u_2^2$. This minimization should indirectly reduce muscle activation inputs as virtual controls are muscle contraction velocities. Similar to [35], the least square virtual control inputs are given as

$$u_1 = -\frac{\Phi'_{S1}}{\Delta}\beta \tag{108}$$

$$u_2 = \frac{\Phi'_{S2}}{\Delta}\beta \tag{109}$$

where $\Delta = (\Phi'_{S1})^2 + (\Phi'_{S2})^2$.

Remark 4.1: Since nonlinear functions Φ_{Sj}, Φ_{Pj}, f_j, and g_j^{-1} are defined on finite intervals and there are singularities, constrained techniques must be used to prevent a finite escape time.

B. SIMULATION

To illustrate the proposed scheme, we conducted two numerical simulations for a dual muscle system: noise free and noisy cases. The total length of the dual muscle system is $C = Lm_1 + Lm_2 = 5.54$. The mass of the system is $m = 1$. The reference trajectory is chosen as

$$r = 2.6315 + 0.01\sin 0.5\tau.$$

Functions Φ_{Sj}, Φ_{Pj} are chosen as in (17) and (18), [36]. The parameter of (8) is $W = 0.3$. The parameters of (9) are chosen as: $A = 0.25$, $g_{max} = 1.5$. Due to (17), the upper bound of $\Phi_{S2}(x_4) - \Phi_{S1}(x_3)$ is 1.

The uncertainty of the system is

$$\Delta_\Phi(\tau) = 0.005 + 0.005\sin 0.8\tau. \tag{110}$$

The controller parameters in Subsection IV-A are: $K = [0.5774 \quad 1.2198]$, $Q = \begin{bmatrix} 10 & 0 \\ 0 & 10 \end{bmatrix}$, $P = \begin{bmatrix} 21.1284 & 17.3205 \\ 17.3205 & 36.5955 \end{bmatrix}$, $\gamma = 1$.
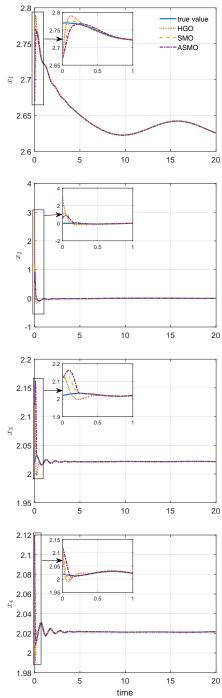

Fig. 4. The true value and estimates of x for the noise free case using 3 observers: high gain observer (HGO), sliding mode observer (SMO), adaptive sliding mode observer (ASMO). All quantities are dimensionless (no units).

The parameters for the high gain observer presented in Section III-A are: $\varepsilon_h = 0.1$, $h_{11} = 3$, $h_{12} = 3$, $h_{13} = 1$, $h_{21} = 2$, $h_{22} = 1$, $h_{31} = 2$, $h_{32} = 1$. As pointed out in Section III-A, h_{11}, h_{12}, h_{13} are chosen such that the polynomial $s^3 + h_{11}s^2 + h_{12}s + h_{13}$ is Hurwitz, and h_{ij} for $i = 2,3$ and $j = 1,2$ are chosen such that the polynomials $s^2 + h_{i1}s + h_{i2}$ are Hurwitz for $i = 2,3$. As the parameter ε_h is small, the convergence speed increases but when there is measurement
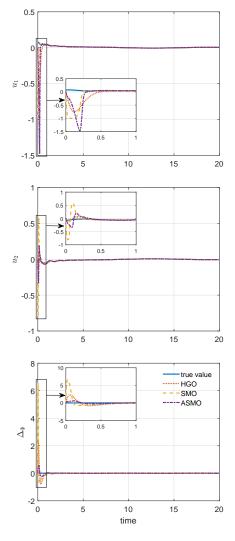
Fig. 5. The true value and estimates of u and Δ_Φ for the noise free case using 3 observers: high gain observer (HGO), sliding mode observer (SMO), adaptive sliding mode observer (ASMO). All quantities are dimensionless (no units).

noise, the performance of the observer is degraded [41], [42]. Hence, ε_h should not be too small.

The parameters for the sliding mode observer presented in Section III-B are: $\alpha_{11} = 1.1$, $\lambda_{11} = 28.17$, $\alpha_2 = 1.1$, $\alpha_3 = 1$, $\tau_s = 0.01$, $\delta_s = 0.01$. The tuning of the parameters was shown in Section III-B, in which α_{11} and λ_{11} are chosen from (51), (52) where $p = 0.5$ and $f^+ = 1$; α_2 and α_3 are chosen from (53) and (54). As δ_s converges to 0, the approximation (65) becomes the ideal function sign, which leads to high sensitivity to measurement noise. Hence, δ_s should not be too small to avoid degradation of the observer.

The parameters for the adaptive sliding mode observer presented in Section III-C are: $\beta_0 = 1.1$, $\alpha_0 = 2\sqrt{2\beta_0} = 2.97$, $\eta_1 = 0.2$, $\eta_2 = 0.2$, $a = 0.82$, $l_0 = 0.4$, $r_{00} = 0.4$, $r_{01} = 0.5$, $r_{02} = 0.5$, $\tau_a = 0.01$, $\varepsilon_{a1} = 0.2$, $\varepsilon_{a2} = 0.2$, $\alpha_{a1} = 0.99$, $\alpha_{a2} = 0.99$, $\gamma_{a0} = 200$, $\gamma_{a1} = \gamma_{a2} = 300$, $\delta_{00} = \delta_{01} = \delta_{02} = 0.001$, $\delta_a = 0.01$. The parameters of β_0 and α_0 are chosen according to [27] where $\alpha_0 = 2\sqrt{2\beta_0}$; eta_1 and η_2 in (69) and (71) are chosen as small numbers [26]; a in (76) is chosen such as
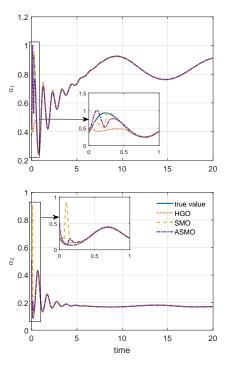

Fig. 6. The true value and estimates of a for the noisy case using 3 observers: high gain observer (HGO), sliding mode observer (SMO), adaptive sliding mode observer (ASMO). All quantities are dimensionless (no units).

$0 < a < 1/\beta_0 < 1$ [27]; l_0 in (78) and r_{00} in (80) are chosen as small positive values [27]; r_{01} and r_{02} in (85) are small positive parameters [26]; τ_a in lowpass filters (68), (70), (72) are chosen to be small; ε_{aj} and α_{aj} ($j = 1, 2$) are chosen such that $0 < \alpha_{aj} < 1$ and $\varepsilon_{aj} > 0$ to satisfy (83); γ_{a0} in (81) and γ_{aj} in (86) ($j = 1, 2$) are positive; δ_{00} in (81) and δ_{0j} ($j = 1, 2$) in (86) are small positive numbers; δ_a of the approximation function of the sign function in (93) is a small positive number. Similar to the sliding mode observer above, if δ_a is too close to 0, the observer will become degraded as this parameter is sensitive to measurement noise.

Note that the model under consideration is dimensionless as pointed out in Section II. Hence, there are no units specified on axes in the following figures.

In the first simulation, no noise affects the measurements of the system output. In Fig. 3, due to the presence of the uncertainty $\Delta_\Phi(\tau)$, x_1 is only able to be close to the reference signal after $\tau = 8$, which demonstrates that the tracking control law is effective in producing a good tracking performance. It is shown in Fig. 4 that the estimates of x_1, x_2, x_3, x_4 using the three observers converge to their true value at about $\tau = 0.5$. The estimates using the high gain observer experience peaks during transients. Fig. 5 depicts the evolution of the estimates of the uncertainty Δ_Φ and unknown inputs u_1 and u_2, which track well their true values. The estimates of the activation signals shown in Fig. 6 converge to their true values. The closeness of the estimates and their true values reveals that the estimation schemes are effective in estimating the state variables and activation signals.

Next, the second simulation was conducted when the measurements were influenced by noise. The noise affecting the
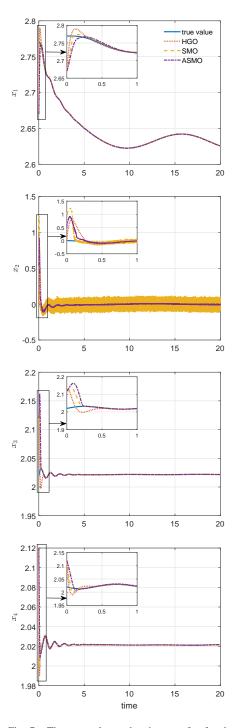
Fig. 7. The true value and estimates of x for the noise free case using 3 observers: high gain observer (HGO), sliding mode observer (SMO), adaptive sliding mode observer (ASMO). All quantities are dimensionless (no units).

Fig. 8. The true value and estimates of u and Δ_Φ for the noisy case using 3 observers: high gain observer (HGO), sliding mode observer (SMO), adaptive sliding mode observer (ASMO). All quantities are dimensionless (no units).

measurement signal of x_1 is uniformly distributed in the interval $[-0.001, 0.001]$ and sampling time $T_s = 0.005$. The measurements of the forces $\Phi_{S1}(x_3)$ and $\Phi_{S2}(x_4)$ are influenced by a noise profile which is a sum of a drift term of 0.001 and values uniformly distributed in the interval $[-0.001, 0.001]$ with sampling time $T_s = 0.005$. The estimates of x in Fig. 7 look quite close to their counterparts in the noise free case (Fig. 4). Similarly, under the influence of the uncertainty
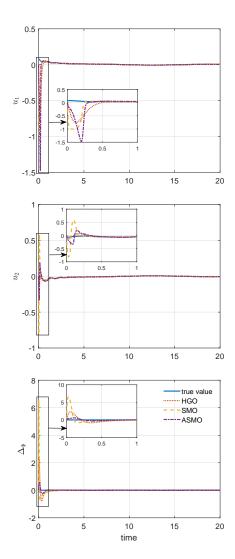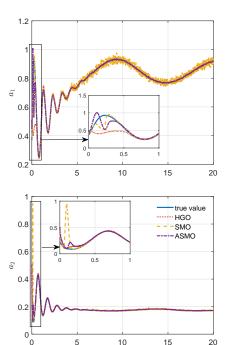
$\Delta_\Phi(\tau)$, x_1 is close to the reference signal after $\tau = 8$. The effect of measurement noise is much clearer in the evolutions of the estimates of x_2 in Fig. 7. Here the estimate of x_2 using the adaptive sliding mode observer is slightly better than the two other observers. In Fig. 8, the estimates of Δ_Φ, u_1, and u_2 look a bit worse than in the noise free case (Fig. 5). The evolutions of the estimates of the activation signals in Fig. 9 track well the true signals. It is shown that the estimates using the adaptive sliding mode observer are closest to the true values. These simulations demonstrate that our proposed estimation schemes produce reliable estimates of the state variables and activation signals in the presence of noise.

The two simulations illustrate that the three observers are comparably effective in estimating the state variables and activation signals of the dual muscle system. Note that the three observers have a lot of freedom in tuning parameters. While the adaptive sliding mode observer does not require knowledge of the bounds of the unknown inputs and uncertainty, the sliding mode observer offers more simple tuning with fewer

Fig. 9. The true value and estimates of *a* for the noisy case using 3 observers: high gain observer (HGO), sliding mode observer (SMO), adaptive sliding mode observer (ASMO). All quantities are dimensionless (no units).

parameters.

V. CONCLUSIONS

In this paper, we have presented the agonistic-antagonistic muscle system based on the Hill muscle model. Three estimation approaches have been introduced to estimate the state variables and activation signals. The high gain observer is constructed based on recent development of the high gain estimation approach [22], [23]. The sliding mode observer is designed based on the super twisting algorithm and first-order sliding mode [19], [34]. The adaptive sliding mode observer is developed based on dual layer adaptive sliding mode schemes presented in [26], [27]. Two numerical simulations were conducted to demonstrate the efficiency of the proposed schemes.

The traditional sliding mode observer is the most simple of the three observers with the least number of parameters but it requires the knowledge of the bounds of the uncertainty and unknown inputs. In contrast, the adaptive sliding mode observer estimates the system in an adaptive way without knowing the information of the uncertainty and unknown inputs at the cost of complexity. The high gain observer provides a flexible approach to observing the system. It was shown that the three observers are comparable through theoretical analysis and simulation results.

Our future work will investigate the estimation problem of more complicated multi-muscle multi-joint systems. In addition, experimental tests will be carried out to validate the proposed estimation schemes.

REFERENCES

[1] Q. Wang, N. Sharma, M. Johnson, C. M. Gregory, and W. E. Dixon, "Adaptive inverse optimal neuromuscular electrical stimulation," *IEEE Transactions on Cybernetics*, vol. 43, no. 6, pp. 1710–1718, Dec 2013.

[2] J. Leaman and H. M. La, "A comprehensive review of smart wheelchairs: Past, present, and future," *IEEE Transactions on Human-Machine Systems*, vol. 47, no. 4, pp. 486–499, Aug 2017.

[3] D. C. Lin, D. Godbout, and A. N. Vasavada, "Assessing the perception of human-like mechanical impedance for robotic systems," *IEEE Transactions on Human-Machine Systems*, vol. 43, no. 5, pp. 479–486, Sept 2013.

[4] X. Xiong, F. Wörgötter, and P. Manoonpong, "Adaptive and energy efficient walking in a hexapod robot under neuromechanical control and sensorimotor learning," *IEEE Transactions on Cybernetics*, vol. 46, no. 11, pp. 2521–2534, Nov 2016.

[5] Y. Na, C. Choi, H. D. Lee, and J. Kim, "A study on estimation of joint force through isometric index finger abduction with the help of semg peaks for biomedical applications," *IEEE Transactions on Cybernetics*, vol. 46, no. 1, pp. 2–8, Jan 2016.

[6] F. E. Zajac, "Muscle and tendon: properties, models, scaling, and application to biomechanics and motor," *Critical Reviews in Biomedical Engineering*, vol. 17, no. 4, pp. 359–411, 1989.

[7] J. M. Winters, *Hill–Based Muscle Models: A Systems Engineering Perspective*. Springer, 1990, ch. 5, pp. 69–93.

[8] H. E. Huxley, "The double array of filaments in cross–striated muscle," *Journal of Biophysical and Biochemical Cytology*, vol. 3, no. 5, pp. 631–648, 1957.

[9] C. A. Yucesoy, B. H. Koopman, P. A. Huijing, and H. J. Grootenboer, "Three–dimensional finite element modeling of skeletal muscle using a two–domain approach: linked fiber-matrix mesh model," *Journal of Biomechanics*, vol. 35, no. 9, pp. 1253–1262, September 2002.

[10] B. Huang, Z. Li, X. Wu, A. Ajoudani, A. Bicchi, and J. Liu, "Coordination control of a dual-arm exoskeleton robot using human impedance transfer skills," *IEEE Transactions on Systems, Man, and Cybernetics: Systems*, vol. PP, no. 99, pp. 1–10, 2017.

[11] T. S. Buchanan, D. G. Lloyd, K. Manal, and T. F. Besier, "Neuromusculoskeletal modeling: estimation of muscle forces and joint moments and movements from measurements of neural command," *Journal of Applied Biomechanics*, vol. 20, no. 4, p. 367, 2004.

[12] A. Erdemir, S. McLean, W. Herzog, and A. J. van den Bogert, "Model-based estimation of muscle forces exerted during movements," *Clinical Biomechanics*, vol. 22, no. 2, pp. 131 – 154, 2007.

[13] S. Mohammed, W. Huo, J. Huang, H. Rifaï, and Y. Amirat, "Nonlinear disturbance observer based sliding mode control of a human-driven knee joint orthosis," *Robot. Auton. Syst.*, vol. 75, no. PA, pp. 41–49, Jan. 2016.

[14] T. Yamasaki, K. Idehara, and X. Xin, "Estimation of muscle activity using higher-order derivatives, static optimization, and forward-inverse dynamics," *Journal of Biomechanics*, vol. 49, no. 10, pp. 2015 – 2022, 2016.

[15] Y.-C. Lin, J. P. Walter, S. A. Banks, M. G. Pandy, and B. J. Fregly, "Simultaneous prediction of muscle and contact forces in the knee during gait," *Journal of Biomechanics*, vol. 43, no. 5, pp. 945 – 952, 2010.

[16] L. Zhao, Q. Li, B. Liu, and H. Cheng, "Trajectory tracking control of a one degree of freedom manipulator based on a switched sliding mode controller with a novel extended state observer framework," *IEEE Transactions on Systems, Man, and Cybernetics: Systems*, vol. PP, no. 99, pp. 1–9, 2017.

[17] A. N. Atassi and H. K. Khalil, "A separation principle for the stabilization of a class of nonlinear systems," *IEEE Transactions on Automatic Control*, vol. 44, no. 9, pp. 1672–1687, Sep 1999.

[18] C. Edwards, S. K. Spurgeon, and R. J. Patton, "Sliding mode observers for fault detection and isolation," *Automatica*, vol. 36, no. 4, pp. 541 – 553, 2000.

[19] J. Davila, L. Fridman, and A. Levant, "Second-order sliding-mode observer for mechanical systems," *IEEE Transactions on Automatic Control*, vol. 50, no. 11, pp. 1785–1789, 2005.

[20] X.-G. Yan and C. Edwards, "Nonlinear robust fault reconstruction and estimation using a sliding mode observer," *Automatica*, vol. 43, no. 9, pp. 1605 – 1614, 2007.

[21] H. Alwi, C. Edwards, and C. P. Tan, "Sliding mode estimation schemes for incipient sensor faults," *Automatica*, vol. 45, no. 7, pp. 1679 – 1685, 2009.

[22] J. Lee, R. Mukherjee, and H. K. Khalil, "Output feedback stabilization of inverted pendulum on a cart in the presence of uncertainties," *Automatica*, vol. 54, pp. 146 – 157, 2015.

[23] ——, "Output feedback performance recovery in the presence of uncertainties," *Systems & Control Letters*, vol. 90, pp. 31 – 37, 2016.

[24] Y. Hou, F. Zhu, X. Zhao, and S. Guo, "Observer design and unknown input reconstruction for a class of switched descriptor systems," *IEEE Transactions on Systems, Man, and Cybernetics: Systems*, vol. PP, no. 99, pp. 1–9, 2017.

[25] W. He, A. O. David, Z. Yin, and C. Sun, "Neural network control of a robotic manipulator with input deadzone and output constraint," *IEEE Transactions on Systems, Man, and Cybernetics: Systems*, vol. 46, no. 6, pp. 759–770, June 2016.

[26] C. Edwards and Y. B. Shtessel, "Adaptive continuous higher order sliding mode control," *Automatica*, vol. 65, pp. 183 – 190, 2016.

[27] C. Edwards and Y. Shtessel, "Adaptive dual-layer super-twisting control and observation," *International Journal of Control*, vol. 89, no. 9, pp. 1759–1766, 2016.

[28] L. Nguyen, H. M. La, and T. H. Duong, "Dynamic human gait phase detection algorithm," in *Proc. of The ISSAT International Conference on Modeling of Complex Systems and Environments (MCSE)*, June 2015, pp. 1–5.

[29] J. Juen, Q. Cheng, V. Prieto-Centurion, J. A. Krishnan, and B. Schatz, "Health monitors for chronic disease by gait analysis with mobile phones," *Telemedicine and e-Health*, vol. 20, no. 11, pp. 1035–1041, 2014.

[30] J. P. Azulay, C. Van Den Brand, D. Mestre, O. Blin, I. Sangla, J. Pouget, and G. Serratrice, "Automatic motion analysis of gait in patients with parkinson disease: effects of levodopa and visual stimulations," *Revue neurologique*, vol. 152, no. 2, pp. 128–134, 1996.

[31] Q. Yuan and I. M. Chen, "3-d localization of human based on an inertial capture system," *IEEE Transactions on Robotics*, vol. 29, no. 3, pp. 806–812, June 2013.

[32] L. V. Nguyen and H. M. La, "Real-time human foot motion localization algorithm with dynamic speed," *IEEE Transactions on Human-Machine Systems*, vol. 46, no. 6, pp. 822–833, Dec 2016.

[33] ——, "A human foot motion localization algorithm using imu," in *2016 American Control Conference (ACC)*, July 2016, pp. 4379–4384.

[34] C. Edwards and S. Spurgeon, *Sliding Mode Control: Theory and Applications*.   CRC Press, 1998.

[35] H. Richter and H. Warner, "Backstepping control of a muscle-driven linkage," in *Proceedings of the 2017 IFAC World Congress*, 2017.

[36] H. Warner and H. Richter, "Non-dimensional modeling and simulation of an agonist-antagonist muscle-driven system," Cleveland State University, Department of Mechanical Engineering, Tech. Rep., Oct 2016, available at http://academic.csuohio.edu/richter_h/lab/simulationReport.pdf.

[37] R. Hermann and A. Krener, "Nonlinear controllability and observability," *IEEE Transactions on Automatic Control*, vol. 22, no. 5, pp. 728–740, Oct 1977.

[38] J. A. Moreno and M. Osorio, "Strict Lyapunov functions for the super-twisting algorithm," *IEEE Transactions on Automatic Control*, vol. 57, no. 4, pp. 1035–1040, April 2012.

[39] H. Warner, H. Richter, and A. Van Den Bogert, "Nonlinear tracking control of an antagonistic muscle pair actuated system," in *Proceedings of the 2017 ASME Dynamic Systems and Control Conference*, Tyson Corners, VA, 2017.

[40] A. C. Woods and H. M. La, "A novel potential field controller for use on aerial robots," *IEEE Transactions on Systems, Man, and Cybernetics: Systems*, vol. PP, no. 99, pp. 1–12, 2017.

[41] A. A. Prasov and H. K. Khalil, "A nonlinear high-gain observer for systems with measurement noise in a feedback control framework," *IEEE Transactions on Automatic Control*, vol. 58, no. 3, pp. 569–580, March 2013.

[42] J. H. Ahrens and H. K. Khalil, "High-gain observers in the presence of measurement noise: A switched-gain approach," *Automatica*, vol. 45, no. 4, pp. 936 – 943, 2009.